

PCCP

Threshold Photoelectron Spectroscopy of Organosulfur Radicals

Journal:	Physical Chemistry Chemical Physics		
Manuscript ID	CP-ART-10-2024-003906.R1		
Article Type:	Paper		
Date Submitted by the Author:	31-Oct-2024		
Complete List of Authors:	Karaev, Emil; Universitaet Wuerzburg, Institut fuer Physikalische und Theoretische Chemie Gerlach, Marius; Universität Würzburg, Institut für physikalische und theoretische Chemie Schaffner, Dorothee; Universitaet Wuerzburg, Institut fuer Physikalische und Theoretische Chemie Chemie Hemberger, Patrick; Paul Scherrer Institut, Swiss Light Source Dutton, Sarah; California Institute of Technology, Chemistry Phillips, Maggie; Middlebury College, Vasiliou, AnGayle; MIT, Chemical Engineering; Middlebury College, Fischer, Ingo; Universitaet Wuerzburg, Institut fuer Physikalische und Theoretische Chemie Chemie; Universität Würzburg,		

SCHOLARONE™ Manuscripts



ARTICLE TYPE

Cite this: DOI: 00.0000/xxxxxxxxxx

Threshold Photoelectron Spectroscopy of Organosulfur Radicals

Emil Karaev,^a Marius Gerlach,^a Dorothee Schaffner,^a Sarah E. Dutton,^b Maggie D. Phillips,^b Patrick Hemberger^{*c}, AnGayle K. Vasiliou,^{*b} and Ingo Fischer^{*a}

Received Date Accepted Date

DOI: 00.0000/xxxxxxxxxx

We report vibrationally resolved threshold photoelectron spectra of several sulfur-containing reactive intermediates. This includes the organosulfur radicals CH_2S , CH_3S , CH_2SH , CH_3S_2 , and S_2H , which are relevant in atmospheric chemistry and in astrochemical settings. Due to the high reactivity, the radicals were prepared *in-situ* via pyrolysis of $(CH_3)_2S_2$. The organosulfur species were characterized by photoion mass-selected threshold photoelectron spectroscopy, employing the photoelectron-photoion coincidence setup (PEPICO) and synchrotron radiation from the Swiss Light Source. We report improved ionization energies and characterize ionic ground and excited states, both singlet and triplet. The vibrational structure was simulated based on computed geometries and vibrational frequencies, giving insight into the geometry change upon ionization.

1 Introduction

In this manuscript we present vibrationally resolved photoelectron spectra of the organosulfur radicals CH₃S (methylthio), CH₂SH (mercaptomethyl), CH₂S (thioformaldehyde) and CH₃S₂, (methylperthiyl) as well as of HS₂ (thiosulfeno). In addition spectra of CH₃SH and S₂ confirm previous work. The chemistry of organosulfur radicals is of considerable relevance in astrochemistry, atmospheric chemistry and combustion science. In the atmosphere, sulfur compounds are linked to phenomena like acid rain or ozone destruction. 1 They are partially emitted from natural sources. Dimethyl sulfide, CH3SCH3 is for example produced by phytoplankton in surface water and released into the atmosphere. 2 Volcanic emissions are a further natural source. 3 However, the main source of sulfur compounds in the atmosphere are anthropogenic activities, in particular burning coal. 4 Compounds like dimethylsulfide or dimethyldisulfide, CH₃SSCH₃ have considerable absorption cross sections in the UV and are precursors to species like the methylthio radical CH₃S that is further oxydized to methylthio peroxy radical, CH₃SOO.⁵

Astrochemistry is another field where sulfur chemistry is not well understood, and a large number of stable as well as reactive species have been detected. Sulfur-containing molecules are much less abundant in dense molecular clouds than expected from the overall cosmic abundance, so main reservoirs are still

It is thus not surprising that considerable efforts have been dedicated to the spectroscopic characterization of isolated Scontaining reactive molecules, in particular CH₃S. Microwave⁹ and infrared 10 spectra of this radical have been reported in the gas phase. The kinetics of R + O2 reactions has been studied (R=CH₃S,...)⁵ and the photochemistry and photodissociation dynamics of CH₃S has been reported using photofragment translational energy spectroscopy 11 and high-n Rydberg H-atom timeof-flight spectroscopy. 12 Negative ion photoelectron spectra revealed the ground state structure and an electron affinity (EA) of 1.861 eV. 13 The photodissociation of CH3S2 was found to yield CH_3 + S_2 as well as CH_3S + $S.^{14}$ Photoion efficiency curves and photoelectron spectra of CH₃S, 15,16 CH₂S, 17,18 CH₃SH 15 and CH₃S₂ 19 using He(I) lamps as a light source have been reported and yielded ionization energies (IE), but the instrument resolution did not allow to fully resolve the vibrational structure. For the thiosulfeno radical S2H, a number of computational studies ^{20,21} as well as a microwave spectrum ²² have been reported. but data on the ion is not available. The available IE values are summarized in Table 1. However, the determination of thermochemical quantities like dissociation energies or heats of for-

E-mail: ingo.fischer@uni-wuerzburg.de

unknown. Thus improved reaction networks are in demand, aiming at a better description of sulfur chemistry in space and including more relevant species. Such a network was just published for the mercaptomethyl radical CH₂SH in the interstellar medium. ⁷ Recently, the James Webb space telescope (JWST) detected SO₂ as an atmospheric component of the exoplanet WASP-39b, ⁸ which confirms that understanding sulfur chemistry will be relevant for understanding processes in exoplanetary atmospheres as well.

 $^{^{\}rm a}$ University of Würzburg, Institute of Physical and Theoretical Chemistry, Am Hubland, 97074 Würzburg, Germany

 $^{^{}c}$ Paul Scherrer Institute, Villigen 5232, Switzerland, e-mail: patrick.hemberger@psi.ch

b Middlebury College Department of Chemistry and Biochemistry, Middlebury VT 05753, e-mail: avasiliou@middlebury.edu

mation requires accurate IEs. Furthermore, photoionization and photoelectron spectroscopy using tunable VUV radiation is now developing into a tool to detect and identify reaction products. ²³ Therefore, there is increasing demand for vibrationally resolved photoelectron spectra. As such quantitative information is lacking for many relevant sulfur species, we initated a study aimed at investigating organosulfur radicals and biradicals using tunable synchrotron radiation at the Swiss Light Source (SLS). Threshold photoelectron-photoion coincidence spectroscopy (TPEPICO) is employed, ²⁴ which permits to record ion mass-selected threshold photoelectron (ms TPE-) spectra. This approach has been demonstrated to be well-suited for studies on reactive intermediates. 25 It is also relevant for identification of reactive species in interstellar space, as recently shown for CH₃. ^{26,27} So far, vibrationally resolved TPE-spectra have only been reported for a few sulfur containing species, including S₂. ²⁸

2 Methods

2.1 Experimental

All experiments were carried out at the VUV beamline of the Swiss Light Source (SLS) at the Paul-Scherrer Institute, Villigen/CH. The double imaging photoelectron photoion coincidence setup CRF-PEPICO was employed. A detailed description of the setup was already published, $^{29-32}$ therefore only a brief description is given here. Synchrotron radiation was provided by a bending magnet, collimated by a mirror and then vertically dispersed by a 150 l/mm plane grating. The light is then guided through a Ne/Ar/Kr gas mixture to filter out higher harmonics of the radiation. The photon energy was calibrated on the 11 s'-13 s' autoionization lines of argon in both the first and second order of the grating. It shows that a spectral resolution of 5 meV has been achieved at 7.882 eV.

The precursor dimethyldisulfide S₂(CH₃)₂ was purchased from ABCR. The reactive species were generated in a Chen type pyrolysis reactor³³ by passing the vapor of the precursor diluted in Argon through a resistively heated SiC tube. The pyrolysis products then enter the experimental chamber through a 2 mm skimmer. There, the molecular beam crosses the synchrotron radiation and the species are ionized. The resulting photoelectrons and photoions were extracted in opposite directions in a constant electric field of 218 V/cm. The photoelectrons were imaged on a Roentdek DLD40 delay line anode detector, while the cations were collected in a Wiley-McLaren type Time of Flight (TOF) spectrometer. Threshold photoelectron were selected by subtracting the contribution of hot electrons from the center of the 2D newton sphere. 34 Photoions and threshold electrons were detected in coincidence, using a multiple-start/multiplestop scheme. 35 Hemberger et al. previously showed that the contributions from re-thermalized ions can be distinguished from effusive beam contributions by velocity map imaging (VMI).³⁶ We followed this approach and only selected ions that were re-thermalized by wall collisions. As a result, the TPE spectra presented below correspond to room temperature, show only minor contributions from hot bands and yield an improved resolution. All IEs were corrected for the Stark shift.

2.2 Theory

IEs, geometries and vibrational frequencies were computed with the ORCA 37 or Gaussian 1638 program packages. Computational details as well as the calculated geometries and vibrations for all molecule in their relevant electronic state are given in the ESI. Generally, ground states were calculated with the G4 composite method of Gaussian 16, while excited states were calculated on the TD-DFT level with a ωB97X-D3 functional and a cc-pVTZ basis set. IEs were obtained by subtracting the energy of the neutral molecule from the one of the cation, both in their vibrational ground state. Thus zero point energy has been included. The IEs obtained by different composite methods are compared in Table S1. Based on the computed geometries and frequencies, Franck-Condon (FC) factors were simulated with ezSpectrum at 300 K. 39 A Gaussian function was then convolved with the computed stick spectra to obtain the simulated spectra displayed below. The combined error bars for photon (5 meV) and electron resolution (10 meV) is around 11 meV and typically smaller than the band width of the vibrational transitions. The band envelope is well described by a Gaussian function. Hence we use the half width at half maximum (FWHM/2) of the origin transition as the error bar for the ionization energy (IE). Typically, an envelope with a FWHM of 25 meV provided good fit results, which leads to error bars of \pm 0.013 eV for all IEs.

3 Results and Discussion

Table 1 Experimental and calculated ionization energies of the observed molecules in the TOF. The experimental IEs determined in the present work are accurate to within \pm 0.013 eV, with the exception of the b^+ state of CH₃S (± 0.06 eV).

species	transition	IE _{exp.}	$IE_{calc.}$	lit.
		/ eV	/ eV	
$\overline{\text{CH}_3\text{S}_2}$	$X^{+} {}^{1}A' \leftarrow X {}^{2}A''$	8.61	8.60^{a}	$8.62\pm0.05,^{40}$
				$8.63\pm0.02,^{19}$
				8.67 ± 0.03^{41}
	$a^+ {}^3A'' \leftarrow X {}^2A''$	9.17	9.21^{a}	9.36 ¹⁹
	$A^{+1}A'' \leftarrow X^{2}A''$	9.65	9.80^{b}	9.94 ¹⁹
S_2H	$X^{+} {}^{1}A' \leftarrow X {}^{2}A''$	9.22	9.22^{a}	_
-	$a^{+3}A'' \leftarrow X^{2}A''$	9.60	9.61^{a}	_
	$A^{+} {}^{1}A'' \leftarrow X {}^{2}A''$	10.17	10.33^{b}	_
CH_3SH	$X^+ {}^2A'' \leftarrow X {}^1A'$	9.44	9.44 ^a	$9.46,^{42}$ $9.44,^{43}$ 9.42^{44}
Ü				
CH_3S	X^+ $^3A_2 \leftarrow X$ $^2A'$	9.25	9.26^{a}	9.26 ± 0.005^{15}
Ü	-			9.225 ± 0.014^{16}
	$a^{+1}A' \leftarrow X^{2}A'$	_	9.95 ^a	$10.12^{45}, 10.13^{46}$
	$b^{+1}A_1 \leftarrow X^2A''$	10.22	10.26 ^b	10.28 ⁴⁶ (1 ¹ A")
	5 11 11	10.22	10.20	10.20 (111)
CH ₂ SH	$X^{+} {}^{1}A' \leftarrow X {}^{2}A''$	7.55	7.52^{a}	8.04 45
2011		,0		
CH_2S	X^{+} $^{2}B_{2} \leftarrow X$ $^{1}A_{1}$	9.37	9.38^{a}	9.376 ± 0.003 , 17 9.38 18
20	2 , 11 11	,,	,	,, :=:::30, ,.00

^a Calculated by G4

^b Calculated by (TD-)DFT/ωB97X-D3

3.1 Mass spectra

Although pyrolysis can produce radicals rather selectively, a mixture of species is often obtained, in particular in a continuous expansion. Mass spectra recorded at 9.5 eV that show the distribution of reaction products at three different pyrolysis temperatures are presented in Figure 1. To rationalize the mass spectra, dissociative photoionization (DPI) of the precursor CH3SSCH3 to smaller fragments has to be understood, because it can obscure the detection of pyrolysis products. The lowest appearance energy to $CH_3SCH_2^+$ + HS an $E_0 = 10.41$ eV has already been determined in previous work. 47 A breakdown diagram from the present work, which agrees with literature is given in Figure S2 in the ESI. Figure S3 shows mass-selected ion images, which prove that even at a photon energy of 11.5 eV kinetic energy release is almost negligible and the contribution from DPI is small. Hence the mass spectra are not significantly affected by DPI. The presence and amount of sulfur isotopes can be derived from the natural sulfur isotope distribution ³²S (95.02 %) and ³⁴S (4.21 %). Thus the pair of peaks at m/z 94 and 96 is readily assigned to the CH₃SSCH₃ precursor. The further isotopes ³³S (0.75 %) and ³⁶S (0.02 %) are of minor importance here.

Hence, at a photon energy of 9.5 eV and using a room temperature sample only the ionized precursor is visible in the TOF (pyrolysis off, top trace). At a temperature of 650 K in the reactor (center trace), the precursor starts to thermally decompose, lose a methyl group and form m/z 79, $CH_3S_2^+$.

A small amount of m/z 64, i.e. S_2^+ is also formed, corresponding to loss of both methyl groups. At even higher reactor temperatures of 800 K the precursor is almost completely pyrolysed, mainly to S_2^+ and $CH_3S_2^+$. In addition, m/z 46, 47, 48 (CH_2S^+ , CH_3S^+ , CH_3SH^+) are formed. A small amount of dimethyl sulfide (m/z 62) is also produced. The change in the distribution pattern indicates the onset of bimolecular chemistry in the reactor, which will be subject of a future publication. A detailed look at the peak at m/z 65 reveals an unusually high intensity that cannot be explained by the natural abundance of ^{33}S , which is only 0.75 %. Hence we conclude that S_2H^+ does also contribute to the mass signal.

While mass spectrometry only provides information about the elemental composition of the pyrolysis products, TPE spectroscopy permits to derive the structure as well as the electronic states of the species involved. The photoelectron spectrum of the precursor m/z 94 has been discussed before, its ms-TPES is thus only presented in the ESI. ^{48–51} In the next sections, we will discuss the TPE spectra of the various intermediates mostly in the order of decending m/z.

3.2 CH₃S₂

Figure 2 shows the TPE spectrum of m/z 79, which corresponds to the loss of one CH_3 group in the reactor, resulting in $CH_3S_2^+$. Three major bands are observed. While the two higher energy bands starting at around 9.1 and 9.6 eV show resolved vibrational structure, the lowest one between 8.5 eV and 8.9 eV displays only little structure. Simulations based on computed geometries and IEs can provide further insight. Neutral CH_3S_2 in its electronic

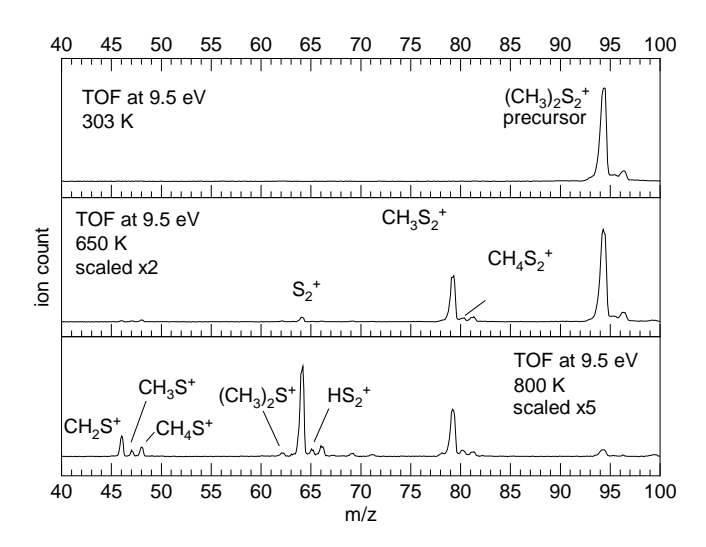


Fig. 1 TOF mass spectra at 9.5 eV photon energy, recorded at reactor temperatures of 303 K, 650 K and 803 K. At room temperature only the precursor $\mathsf{CH}_3\mathsf{SSCH}_3$ is present. At higher pyrolysis temperature the precursor dissociates and different sulfur species are formed.

ground state has C_s symmetry with one unpaired electron sitting in an a" molecular orbital (MO), which resembles a π^* orbital. According to the computations, the IE for the X^{+} $^{1}A' \leftarrow X$ $^{2}A''$ transition to the electronic ground state of the cation is 8.60 eV, as found by G4, which matches the shape of the lowest energy band. The red line represents a simulation based on computed Franck-Condon factors, which fits the TPE spectrum quite well. An IE of 8.61 \pm 0.013 eV is derived, in agreement with values reported before. 19,40,41 The broad and only partially resolved band is indicative of a large geometry change upon ionization. Computations show that the S-S bond length shortens by 0.09 Å (4 %), from 1.95 Å to 1.86 Å while the S-C bond length shortens only by 0.02 Å (1 %). In contrast, the S-S-C bond angle increases by 5° (5 %). As a consequence, combination bands and overtones of $v_9^+ = 730 \text{ cm}^{-1} \text{ (C-S-S stretching mode)}, v_{10}^+ = 630 \text{ cm}^{-1} \text{ (C-}$ S stretching mode) and $v_{11}^+ = 280 \text{ cm}^{-1}$ (C–S–S bending mode) are excited. Note that in the simulations, the internal rotation of the methyl group has been neglected, which introduces further broadening.

The second band from 9.0 – 9.4 eV is assigned to the transition into the first triplet excited state a^+ $^3a'' \leftarrow X$ $^2A''$. In this transition, the electron is removed from the HOMO–1 (second highest occupied molecular orbital). This nominally nonbonding orbital also has some ressemblance with a S–S or S-C π^* MO, but in this case with a' symmetry. In contrast to the $^1A'$ state, the S–S bond length changes in this state only slightly by 0.01 Å (0.5 %), which results in negligible excitation of the S–S stretching mode. Thus, the geometry change upon ionization is small, leading to a well defined origin transition, which is followed by excitations of $v_{10}^+ = 620 \text{ cm}^{-1}$ (C–S stretching mode), $v_7^+ = 980 \text{ cm}^{-1}$ (CH₃ wagging mode) and $v_6^+ = 1350 \text{ cm}^{-1}$ (CH₃ umbrella mode) fundamentals. The experimental IE of 9.17 \pm 0.013 eV is in agreement with the one of 9.21 eV calculated by G4. In comparison with previous data the IE differs by 0.19 eV. 19 However, only the

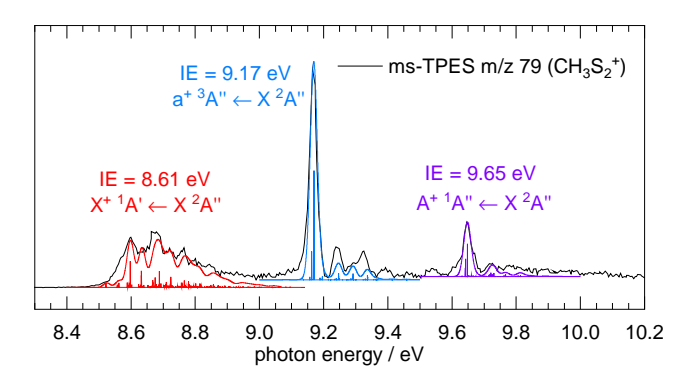


Fig. 2 ms-TPE spectrum of m/z 79, which corresponds to the molecule CH₃S₂⁺. From the neutral $^2A^{\prime\prime}$ ground state transitions into the cationic ground state X⁺ $^1A^{\prime}$ (red FC simulation), the lowest cationic triplet state a⁺ $^3A^{\prime\prime}$ (purple FC simulation) and the A⁺ $^1A^{\prime\prime}$ (blue FC simulation) are observed. Note that the baseline of the two latter transitions is higher due background signals.

band maximum was reported in this earlier work.

The third band from 9.5 – 9.9 eV results from ionization of an electron from the same π^* -like a' orbital but terminating in an excited singlet state of the ion. The IE of this A^+ $^1A' \leftarrow X^2A''$ transition was calculated to be 9.80 eV. The experimental IE is determined to be 9.65 \pm 0.013 eV. The value is thus 0.19 eV lower than the previously reported band maximum. 19 The FC simulation mainly shows activity in the $v_{10}^+ = 590$ cm $^{-1}$ (C–S stretching mode), $v_9^+ = 660$ cm $^{-1}$ (S–S stretching mode) and $v_6^+ = 1350$ cm $^{-1}$ (CH₃ umbrella mode).

The calculated and experimental IEs of CH_3S_2 as well as of all other investigated species are summarised and compared with available literature values in Table 1 and Table S1 (ESI).

3.3 S₂H

From CH₃S₂, an abstraction of the remaining methyl group leads to S2, which yields the most intense signal in the TOF at m/z 64 and 66. Its slow photoelectron spectrum has already been analyzed in detail by Hrodmarsson et al., 28 which is in excellent agreement with the TPES shown in the black trace of figure 3a). We therefore refrain from a detailed discussion, but note that our value of 9.35 eV for the transition into the $X^2\Pi_{1/2}$ ground state of the ion compares well with the previous value of 9.371 eV. In the TOF spectrum, an additional signal is present at m/z 65, which is not only due to the ³³S isotopologue of S₂, but also contains contributions from the thiosulfeno radical S2H. The blue trace shows the TPES recorded for m/z 65. It is evident that several bands are identical to bands observed for m/z 64 and thus have to be assigned to ³²S³³S, but additional bands are visible that are due to S₂H. By normalizing the spectra at m/z 64 and 65 to the $a^4\Pi_u$ state of S_2^+ (not shown) and subtracting them, the spectrum in figure 3 b) is obtained. An additional progression around 9.6 eV becomes apparent, as well as some smaller features around 9.3 eV. These features are assigned to the S2H radical. S₂H has only recently been observed in the horsehead nebula, 52 and thus attracts astrochemical interest. G4 calculations

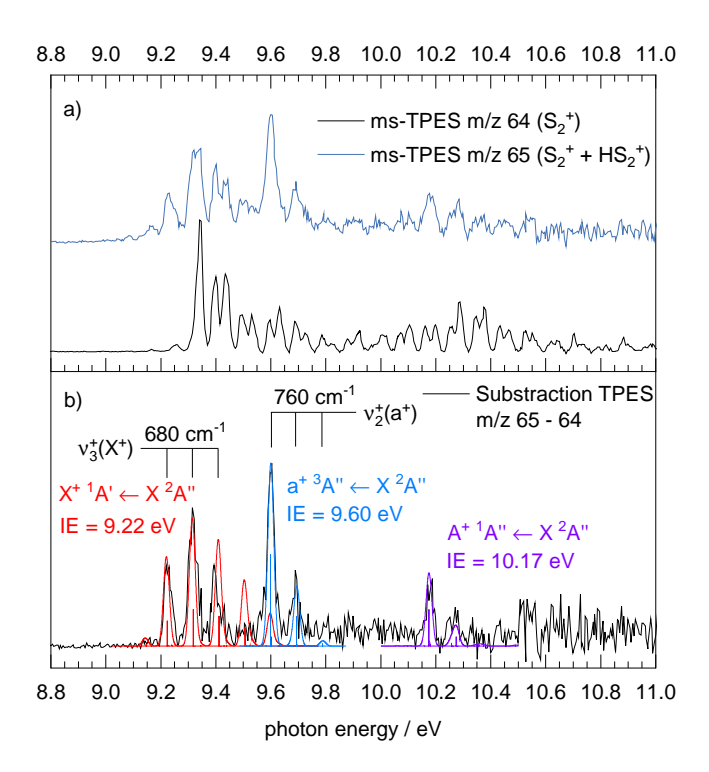


Fig. 3 a) ms-TPES of m/z 64 (S_2^+ , black) and of m/z 65 ($S_2^- + S_2^- H^+$, blue) b) subtraction spectrum m/z 65 – m/z 64. The spectra were normalized on the $a^+ \, ^4\Pi_u$ band of S_2^+ (not shown). The FC simulations of the $X^+ \, ^1A'$, $a^+ \, ^3A''$ and $A^+ \, ^1A''$ states are shown in red, purple and blue, respectively.

of S_2H support the assignment of the bands. No information on its cation is yet available. S_2H in its neutral ground state, as well as in its three lowest lying cationic states is bent and exhibits C_s symmetry. Ionization from the a'' (S–S π^* -like) SOMO requires 9.22 ± 0.013 eV and is associated with a reduction of the S–S bond by 0.09 Å (5 %). Therefore a progression in the S–S stretching mode v_3^+ is expected and visible in the spectrum with several overtones. A wavenumber of 680 cm⁻¹ is obtained from the data. The simulated spectrum of the $X^{+1}A' \leftarrow X^{2}A''$ transition (red trace in Figure 3b) represents the experimental one quite well.

Ionization from the lower lying a' (also π^* -like) orbital forms two cationic states, with the a^{+ 3}A" triplet state being lower in energy. The light blue line represents a simulation of the a^{+ 3}A" \leftarrow X 2 A' transition. The experimentally derived IE of 9.60 \pm 0.013 eV is in excellent agreement with the value of 9.61 obtained from G4 calculations. The a^{+ 3}A" state is characterized by a S–S–H bond angle reduction of 6° (6 %), hence the S–S–H bending mode v_2^+ = 760 cm⁻¹ is excited and dominates the spectrum.

Finally, the transition into the A⁺ ¹A" state (purple line) requires 10.17 eV. This transition exhibits a much lower intensity compared to those terminating in the X⁺ and a⁺ states and only the origin transition is observed. In the simulations, excitations to the fundamental of the S–S stretching mode $v_3^+ = 660 \text{ cm}^{-1}$ and the S–S–H bending mode $v_2^+ = 800 \text{ cm}^{-1}$ appear, but they are close to noise level in the experiment.

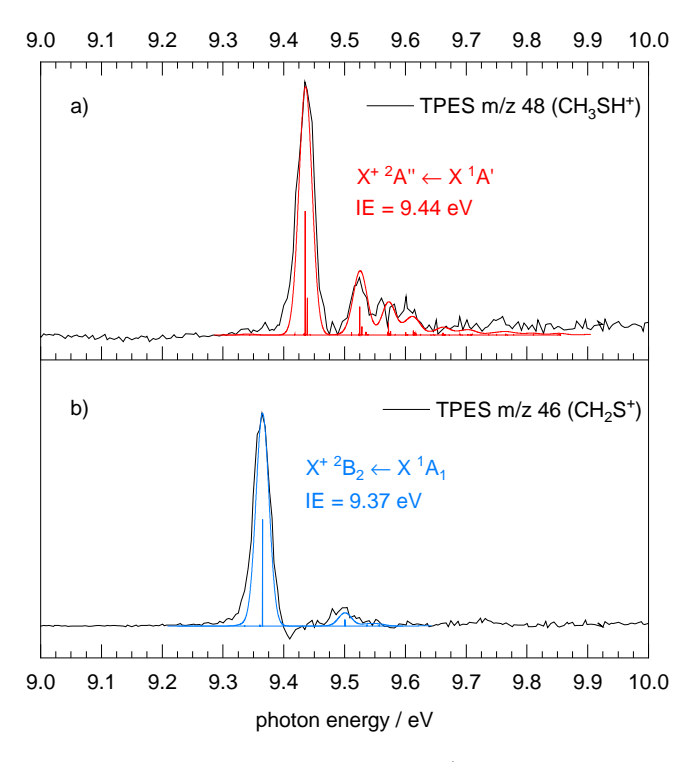


Fig. 4 a) ms-TPE spectra of m/z 48 (CH₃SH⁺). The FC simulation in red describes the X⁺ 2 A" \leftarrow X 2 A' transition. b) ms-TPE spectra of m/z 46 (CH₂S⁺). The blue curve represents the FC simulation of the X⁺ 2 B₂ \leftarrow X 1 A₁ transition.

3.4 CH₃SH

Figure 4 shows the TPE spectra of organosulfur species with m/z 48, and 46 (CH₃SH and CH₂S). For the TPES of m/z 48, contributions from heavier isotopologues of lower masses have been subtracted. Both compounds show similar ionization energies, which impeded assignments in a previous photoelectron study without mass information. 53 Due to the ion mass selection in the present experiments, more information is derived that permits a solid analysis of the TPE-spectra. The top trace of Figure 4a) shows the ms-TPES of methyl mercaptan, CH₃SH. It is a stable molecule with a ¹A' electronic ground state and is likely formed in a bimolecular reaction in the thermal reactor, for example CH₃S + H. A dispersive PES has previously been recorded with a He(I) lamp, 44 and revealed an IE of 9.42 eV. IEs of 9.44 eV and 9.46 eV were derived in other studies and are all in agreement with our experimental IE of 9.44 \pm 0.013 eV. ^{42,43} According to the computations, the S-C bond changes by only 0.04 Å upon ionization of the a" π^* -like HOMO. Hence, the vibronic structure in the TPES is dominated by a pronounced 0-0 transition, followed by low-intensity excitations of the CH3 scissoring and umbrella modes $v_5^+ = 1440 \text{ cm}^{-1}$ and $v_7^+ = 1330 \text{ cm}^{-1}$. An IE of 9.44 eV is obtained from the origin transition.

3.5 CH₂S

Figure 4b) shows the TPES of thioformaldehyde CH₂S. CH₂S has $C_{2\nu}$ symmetry and a b₂ HOMO of π^* -like appearance. Ioniza-

tion from the HOMO thus leads to an increase of bond order, but the C–S bond length decreases only slightly by 0.02 Å (1 %) and the H–C–H angle increases by 2 ° (2 %). The spectrum is dominated by the origin band of the X⁺ $^2B_2 \leftarrow$ X 1A_1 and an IE of 9.37 \pm 0.013 eV is derived and is in agreement with the calculated IE of 9.38 eV. The IE is in line with the previous values of 9.376 \pm 0.003 eV derived from a PIE curve 17 and 9.38 eV derived from a He(I) PES. 18

Due to the small geometry change upon ionzation, only a short vibrational progression is visible in the simulation (blue line). The C–S stretching mode $v_4^+=1100~{\rm cm}^{-1}$ and the symmetric CH₂ bending mode $v_3^+=1380~{\rm cm}^{-1}$ appear, but cannot be separated in the spectrum. In addition, the symmetric H–C–H stretching mode appears at $v_2^+=3060~{\rm cm}^{-1}$ with very low intensity.

3.6 CH₃S and CH₂SH

Finally, the ms-TPES for m/z 47 is given in Figure 5. Two isomers potentially contribute to the spectrum, the thiomethyl radical CH₃S or the mercaptomethyl radical, CH₂SH. On the potential energy surface of the neutral, CH₃S represents the global minimum. From a thermochemical cycle it was derived to be more stable by 6.3 ± 2 kcal/mol (0.27 eV), while our computations with G4 place it 0.36 eV lower in energy. It is therefore preferentially formed in a thermal reactor. The neutral molecule is C_{3v}-symmetric with three electrons in the π^* orbitals, i.e. $(\pi^*)^3$ occupancy, a 2 E ground state and thus subject to both spin-orbit coupling and Jahn-Teller distortion. The latter induces a symmetry reduction to C_s and splits the 2 E state into a lower energy 2 A' and a higher energy 2 A'' component, as outlined in previous studies. 54 It was found that the Jahn-Teller stabilisation is larger than the spin-orbit splitting (44 meV vs 12 meV). 55

Experimentally, values of $-255.5~\rm cm^{-1}$ (32 meV) and $-221~\rm cm^{-1}$ (27 meV) have been determined for the spin-orbit splitting from laser-induced fluorescence and microwave spectroscopy. 9,56 For the interpretation of the TPE spectrum we assume only transitions from the X 2 A′ state of the thiomethyl radical, although small contributions from thermally populated vibrationally excited states are certainly present.

After ionization of a valence electron, a $(\pi^*)^2$ occupancy remains, giving rise to three electronic states, 3A_2 , 1E and 1A_1 . Hund's rules dictate a triplet ground state for CH₃S⁺, but there has been some confusion whether this state is of 3A_1 , 45,57,58 or 3A_2 symmetry. 59 The 1E state is prone to strong Jahn-Teller distortion since one e orbital is doubly occupied while the other is not. 45 This leads to a strong symmetry reduction to C_s and two new minima arise on the singlet surface, the global X⁺ $^1A'$ mercaptomethyl geometry minimum and a small local minimum with a non-classical bridged hydrogen atom between the sulfur and the CH₂ fragment. 45 In this work, the mercaptomethyl and thiomethyl radical are considered as isomers with separate ground states.

The TPES exhibits a low-intensity vibrational structure around 7.5 eV, which is attributed to the mercaptomethyl radical cation. The calculated IE of 7.52 eV (G4) aligns well with the experimentally observed IE of 7.55 \pm 0.013 eV. Notably, the intensity of

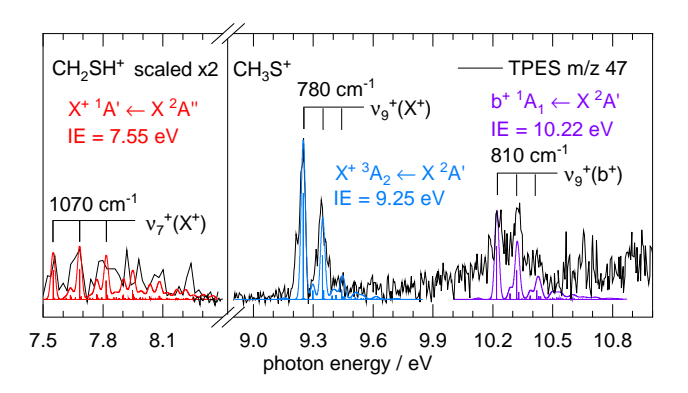


Fig. 5 ms-TPE spectra of m/z 47 (CH₃S⁺ and CH₂SH⁺). The red FC simulation describes the X⁺ 2 A' \leftarrow X 2 A" transition of the CH₂SH isomer. The blue and and purple simulation are both from the CH₃S isomer. The blue shows the transition into the triplet state X⁺ 3 A₂ \leftarrow X 2 A', the purple one into the excited singlet state b⁺ 1 1₁ \leftarrow X⁺ 2 A'

this signal is significantly lower when compared to the signal at 9.2 eV, which is attributed to the CH₃S species. Assuming a Boltzmann distribution and no activation barrier for isomerization at 800 K, the CH₂SH radical would be expected to constitute approximately 2 % of the population (thermochemical cycle). However, since 17 % is observed in the TPES (assuming similar ionization cross sections), we infer that the predominant mechanism for the generation of this radical likely involves a bimolecular reaction between CH₂S and a hydrogen radical. The vibrational progression in the TPES arises through the ionization of an electron in a π^* -like orbital. This increases the bond order between sulfur and carbon, hence leading to a shortening between carbon and sulfur from 1.71 Å in the neutral to 1.61 Å in the cation. This results in an excitation of the S–C stretching mode v_7 ⁺ which has a wavenumber of 1070 cm⁻¹. This progression is accompanied by smaller excitations of v_6^+ and v_8^+ , which are both modes that involve an out of plane hydrogen movement with 1080 cm⁻¹ and 880 cm⁻¹, respectively.

As just mentioned, the signal at 9.25 eV is attributed to the X⁺ 3 A₂ \leftarrow X 2 A′ transition in the isomer CH₃S⁺. The observed IE of 9.25 \pm 0.013 eV agrees well with the calculated IE of 9.21 eV and with the value of 9.225 eV and 9.262 eV obtained in previous photoionization efficiency (PIE) studies. 15,16 Compared to the neutral radical, the X⁺ 3 A₂ state has a shorter S–C bond length. This geometry change leads to excitation of the S–C stretch v_9^+ = 780 cm⁻¹ and the methyl deformation mode v_7^+ = 830 cm⁻¹. The simulation is shown in light blue. From steps in a PIE curve, a vibrational wavenumber of 700 cm⁻¹ was deduced, 15 somewhat smaller, but in reasonable agreement with the present values. Transitions from the spin-orbit excited state of the neutral radical have not been included in the simulation. They might contribute to the width of the vibrational bands that is not fully reflected in the simulations.

A second band with discernible vibrational structure sets in above 10 eV. A previous He(I)-photoelectron study of CH $_3$ S reported bands at 9.91 eV and 10.32 eV and assigned them to a transition into the excited 1E and 1A_1 states of the ion. 60 These

assignments have to be contested. In our data, the band observed at 9.91 eV is absent and probably has to be assigned to a different species. The third band reported at 10.32 eV might match our second band above 10 eV, although the intensities are quite different. The assignment is less than obvious, though. The excited a^{+} 1E state of CH_3S^{+} is subject to Jahn-Teller distortion and will experience a symmetry reduction to C_s . The e (π^*) orbitals split into their a' and a'' components, leading to two A' states since in both cases the orbitals are doubly occupied.

A potential energy surface of the [H₃, C, S]⁺ system was computed using the B3LYP functional, followed by CCSD(T) calculations at the stationary points. 45 It was found that the minimum energy geometry on the singlet surface corresponds to the CH₂SH⁺ isomer in its ¹A' state, confirming prior theoretical studies. In contrast, no minimum for the CH₃S⁺ structure was found on the cationic singlet potential energy surface of the ${}^{1}A'$ state. However, a transition into the b+ 1A1 is possible at this photon energy according to our relaxed potential energy surface scans (figure S4 in the ESI). The calculated ionization energy of the b⁺ ¹A₁ 10.26 eV (TD-DFT) is in agreement with the experimentally observed one of 10.22 \pm 0.06 eV. A progression with a spacing of 810 cm⁻¹ (100 meV) is observed, which is assigned to the S-C stretching mode $v_9^+ = 810 \text{ cm}^{-1}$ of the b⁺ state. The FC simulation is shown in purple. Note that apart from the intensity of the signal, the simulation of the $X^{+3}A_2$ and the $b^{+1}A_1$ are very similar. Reason for that are similar electronic structures. Both species have the same electron configurations except for the flipped spin within the π orbital, which should have a negligible effect on the geometry.

As noted before, a non-classical minimum was found on the potential energy surface of the $^1\mathrm{A'}$ by Aschi *et al.* 45 Our calculations also indicate such a structure. However, since the geometry changes significantly compared to the $^2\mathrm{A'}$ of CH₃S, the Franck-Condon factors are three orders of magnitude smaller compared to the transition into the b⁺ $^1\mathrm{A_1}$ state. Also, the non-classical structure leads to the global minimum CH₂SH barrierless through excitations of v_8^+ and v_9^+ , as can be seen in figure S5 in the ESI. Small contributions within the noise remain possible, though.

3.7 Comparison with oxygen congeners

It is worth comparing the adiabatic IEs (AIE) of the organosulfur radicals to their oxygenated analogs. The AIEs of CH_3S , S_2H , CH_3S_2 are more than 1.4 eV lower, when compared to CH_3O , 61 HO_2 , 62 CH_3O_2 , 63 respectively, which can be rationalized by the higher stabilization of the positive charge in the larger sulfur orbitals, where the electrons are ejected from. In contrast the AIE of CH_2OH^{61} and CH_2SH are almost identical as the radical site is mostly located at the CH_2 group. Understanding the spectroscopy and the electronic structure of the cation as well as determining IEs of organosulfur radicals and cations is crucial as it enables isomer-selective and sensitive detection using mass-spectrometric methods in laboratory experiments. This data can help to develop new approaches to unveil novel formation channels relevant for answering questions in an astro- and atmospheric chemistry context. The experimental and simulated ms-TPE spectra of

the organosulfur species are summarized in the PhotoElectron PhotoIon Spectral COmpendium (PEPISCO) database. ⁶⁴

Conclusion

Threshold photoelectron spectra of small organo-sulfur compounds have been recorded using synchrotron radiation. All species were generated by pyrolysis of dimethyldisulfide. Accurate ionization energies were derived for transitions into the ground state of CH_2S^+ (9.37 eV), CH_3S^+ (9.25 eV), CH_2SH^+ (7.55 eV), CH_3SH^+ (9.44 eV), S_2H^+ (9.22 eV) and CH_3S_2^+ (8.61 eV). In addition, excited electronic states of the cations were characterized for several of the species. The experiments were supported by calculations, which helped to assign the vibrational structure in the spectra.

For CH₂S⁺, CH₃SH⁺ and CH₃S₂⁺ the spectra improve the accuracy of IEs reported in previous work and derived either from band maxima in He(I) photoelectron spectra or from PIE curves. In addition, the hitherto unresolved vibrational structure is resolved. In some cases deviations can be traced back to the difference between adiabatic IEs and band maxima. In the case of CH₃S, however, the ion mass selectivity employed in the present work provides a reliable assignment of bands that is not possible in the He(I) photoelectron spectra. In contrast, S₂H⁺ has not been studied previously. We obtained its photoelectron spectrum by a subtraction procedure, thus distinguishing it from the $^{32}S^{33}S$ isotopologue of S_2 . For the the $X^{+}^{1}A'' \leftarrow X^{2}A'$ transition, an IE=9.22 eV and a wavenumber of 680 cm⁻¹ for the S-S stretching mode were determined. Transitions into the first excited triplet and singlet states were also observed at 9.60 eV and 10.17 eV, respectively.

Acknowledgements

The experiments were performed at the VUV beamline of the Swiss Light Source, located at the Paul Scherrer Institute (PSI). The work was financially supported by the Deutsche Forschungsgemeinschaft, contract FI575/19-1, and by the National Science Foundation (CHE-1566282). DS acknowledges a fellowship by the FCI (Fonds der chemischen Industrie).

Conflict of Interest

There are no conflicts of interest to declare.

Notes and references

- 1 A. Mardyukov and P. R. Schreiner, *Acc. Chem. Res.*, 2018, **51**, 475–483.
- 2 A. Gabric, N. Murray, L. Stone and M. Kohl, *Journal of Geophysical Research: Oceans*, 1993, **98**, 22805–22816.
- 3 C. V. Brodowsky, T. Sukhodolov, G. Chiodo, V. Aquila, S. Bekki, S. S. Dhomse, M. Höpfner, A. Laakso, G. W. Mann, U. Niemeier, G. Pitari, I. Quaglia, E. Rozanov, A. Schmidt, T. Sekiya, S. Tilmes, C. Timmreck, S. Vattioni, D. Visioni, P. Yu, Y. Zhu and T. Peter, Atmos. Chem. Phys., 2024, 24, 5513–5548.
- 4 W. H. Calkins, Fuel, 1994, 73, 475-484.

- 5 J. Chen, T. Berndt, K. H. Møller, J. R. Lane and H. G. Kjaer-gaard, J. Phys. Chem. A, 2021, 125, 8933–8941.
- 6 Lamberts, T., A&A, 2018, 615, L2.
- 7 X. Shao, Z. Wu, L. Wang, G. Rauhut and X. Zeng, *J. Phys. Chem. Lett.*, 2023, **14**, 10450–10456.
- 8 S.-M. Tsai, E. K. Lee, D. Powell, P. Gao, X. Zhang, J. Moses, E. Hébrard, O. Venot, V. Parmentier, S. Jordan *et al.*, *Nature*, 2023, **617**, 483–487.
- 9 Y. Endo, S. Saito and E. Hirota, J. Chem. Phys., 1986, 85, 1770–1777.
- 10 H.-L. Han, L. Fu and Y.-P. Lee, *Chem. Phys. Lett.*, 2011, **515**, 1–6.
- 11 R. T. Bise, H. Choi, H. B. Pedersen, D. H. Mordaunt and D. M. Neumark, *J. Chem. Phys.*, 1999, **110**, 805–816.
- 12 G. Sun, X. Zheng, Y. Song and J. Zhang, *J. Phys. Chem. A*, 2019, **123**, 5849–5858.
- 13 B. K. Janousek and J. I. Brauman, *J. Chem. Phys.*, 1980, **72**, 694–700.
- 14 N. C. Cole-Filipiak, M. Shapero, C. Haibach-Morris and D. M. Neumark, *J. Phys. Chem. A*, 2016, **120**, 4818–4826.
- 15 B. Ruscic and J. Berkowitz, J. Chem. Phys., 1992, 97, 1818– 1823.
- 16 S. Nourbakhsh, K. Norwood, G. He and C. Ng, *J. Am. Chem.Soc.*, 1991, **113**, 6311–6312.
- 17 B. Ruscic and J. Berkowitz, J. Chem. Phys., 1993, 98, 2568– 2579.
- B. Solouki, P. Rosmus and H. Bock, J. Am. Chem. Soc., 1976, 98, 6054–6055.
- 19 G. Maofa, W. Jing, S. Zheng, Z. Xinjiang and W. Dianxun, *J. Chem. Phys.*, 2001, **114**, 3051–3054.
- 20 Q. Zhuo, D. J. Clouthier and J. D. Goddard, J. Chem. Phys., 1994, 100, 2924–2931.
- 21 P. A. Denis, Chem. Phys. Lett., 2006, 422, 434-438.
- 22 M. Tanimoto, T. Klaus, H. S. Müller and G. Winnewisser, *J. Mol. Spectros.*, 2000, **199**, 73–80.
- 23 I. Fischer and S. T. Pratt, *Phys. Chem. Chem. Phys.*, 2022, **24**, 1944–1959.
- 24 T. Baer and R. P. Tuckett, Phys. Chem. Chem. Phys., 2017, 24, 9698–9723.
- I. Fischer and P. Hemberger, ChemPhysChem, 2023, 19, e202300334.
- 26 B. K. Cunha de Miranda, C. Alcaraz, M. Elhanine, B. Noller, P. Hemberger, I. Fischer, G. A. Garcia, H. Soldi-Lose, B. Gans, L. A. Vieira Mendes, S. Boyé-Péronne, S. Douin, J. Zabka and P. Botschwina, J. Phys. Chem. A, 2010, 114, 4818–4830.
- O. Berné, M. Martin-Drumel and I. Schroetter, *Nature*, 2024, 621, 56–59.
- 28 H. R. Hrodmarsson, G. A. Garcia, L. Nahon, J.-C. Loison and B. Gans, *J. Mol. Spectrosc.*, 2021, **381**, 111533.
- 29 M. Johnson, A. Bodi, L. Schulz and T. Gerber, *Nucl. Instrum. Methods Phys. Res. A*, 2009, **610**, 597–603.
- 30 A. Bodi, M. Johnson, T. Gerber, Z. Gengeliczki, B. Sztáray and T. Baer, *Rev. Sci. Instrum.*, 2009, **80**, 034101.

- 31 A. Bodi, P. Hemberger, T. Gerber and B. Sztáray, *Rev. Sci. Instrum.*, 2012, **83**, 083105.
- 32 B. Sztáray, K. Voronova, K. G. Torma, K. J. Covert, A. Bodi, P. Hemberger, T. Gerber and D. L. Osborn, *J. Chem. Phys.*, 2017, **147**, 013944.
- 33 D. W. Kohn, H. Clauberg and P. Chen, *Review of Scientific Instruments*, 1992, **63**, 4003–4005.
- 34 B. Sztáray and T. Baer, Rev. Sci. Instrum., 2003, 74, 3763–3768.
- 35 A. Bodi, B. Sztáray, T. Baer, M. Johnson and T. Gerber, *Rev. Sci. Instrum.*, 2007, **78**, 084102.
- 36 P. Hemberger, X. Wu, Z. Pan and A. Bodi, *The Journal of Physical Chemistry A*, 2022, **126**, 2196–2210.
- 37 F. Neese, F. Wennmohs, U. Becker and C. Riplinger, *J. Chem. Phys.*, 2020, **152**, 224108.
- 38 M. Frisch, G. Trucks, H. Schlegel, G. Scuseria, M. Robb, J. Cheeseman, G. Scalmani, V. Barone, G. Petersson, H. Nakatsuji *et al.*, *Gaussian Inc. Wallingford CT*, 2016, 1, 572.
- 39 S. Gozem and A. I. Krylov, *WIRE Comp. Mol. Sci.*, 2022, **12**, e1546.
- 40 W.-C. Hung, M.-y. Shen, Y.-P. Lee, N.-S. Wang and B.-M. Cheng, *J. Chem. Phys.*, 1996, **105**, 7402–7411.
- 41 Z.-X. Ma, C. Liao, C. Ng, Y.-S. Cheung, W.-K. Li and T. Baer, *J. Chem. Phys.*, 1994, **100**, 4870–4875.
- 42 S.-W. Chiu, W.-K. Li, W.-B. Tzeng and C.-Y. Ng, *J. Chem. Phys.*, 1992, **97**, 6557–6568.
- 43 S. Lias, J. Bartmess, J. Liebman, J. Holmes, R. Levin and W. Mallard, *Monogr.*, 1988, 17, 1.
- 44 D. Frost, F. Herring, A. Katrib, C. McDowell and R. McLean, *J. Phys. Chem.*, 1972, **76**, 1030–1034.
- 45 M. Aschi and F. Grandinetti, *J. Chem. Phys.*, 1999, **111**, 6759–6768
- 46 B. Li, L. Li, Y. Wang and J. Peng, *ACS Omega*, 2020, **5**, 24204–24210.
- 47 S. Borkar, B. Sztáray and A. Bodi, J. Electron Spectrosc. Rel. Phenom., 2014, 196, 165–172.

- 48 W. Li, S. Chiu, Z. Ma, C. Liao and C. Y. Ng, The Journal of Chemical Physics, 1993, 99, 8440–8444.
- 49 J. J. Butler, T. Baer and S. A. Evans Jr, *Journal of the American Chemical Society*, 1983, **105**, 3451–3455.
- 50 S.-Y. Chiang, C.-I. Ma and D.-J. Shr, *The Journal of Chemical Physics*, 1999, **110**, 9056–9063.
- 51 K. Kimura, *Handbook of HeI photoelectron spectra of fundamental organic molecules*, Japan Scientific Society Press, 1981.
- 52 A. Fuente, J. R. Goicoechea, J. Pety, R. L. Gal, R. Martín-Doménech, P. Gratier, V. Guzmán, E. Roueff, J. C. Loison, G. M. M. Caro, V. Wakelam, M. Gerin, P. Riviere-Marichalar and T. Vidal, *ApJ Lett.*, 2017, 851, L49.
- 53 H. Kroto and R. Suffolk, *Chemical Physics Letters*, 1972, **15**, 545–548.
- 54 M. Grütter, J. M. Michaud and F. Merkt, *J. Chem. Phys.*, 2011, **134**, 054308.
- 55 A. V. Marenich and J. E. Boggs, J. Phys. Chem. A, 2004, 108, 10594–10601.
- 56 Y. Hsu, X. Liu and T. A. Miller, *J. Chem. Phys.*, 1989, **90**, 6852–6857.
- 57 R. H. Nobes and L. Radom, *Chem. Phys. Lett.*, 1992, **189**, 554–559.
- 58 L. A. Curtiss, R. H. Nobes, J. A. Pople and L. Radom, *J. Chem. Phys.*, 1992, **97**, 6766–6773.
- 59 J. R. Flores, C. Barrientos and A. Largo, J. Phys. Chem., 1994, 98, 1090–1099.
- 60 X. J. Zhu, M. F. Ge, J. Wang, Z. Sun and D. X. Wang, *Angew. Chem. Int. Ed.*, 2000, **39**, 1940–1943.
- 61 L. A. Curtiss, L. D. Kock and J. A. Pople, *The Journal of Chemical Physics*, 1991, **95**, 4040–4043.
- 62 M. Litorja and B. Ruscic, *Journal of Electron Spectroscopy and Related Phenomena*, 1998, **97**, 131–146.
- 63 Y.-S. Cheung and W.-K. Li, *Journal of Molecular Structure: THEOCHEM*, 1995, **333**, 135–145.
- 64 P. Hemberger, Z. Pan, X. Wu, Z. Zhang, K. Kanayama and A. Bodi, J. Phys. Chem. C, 2023, 127, 16751–16763.

Data Availability Statement

Data for this article will be made available at https://pepisco.psi.ch/pepisco after acceptance of the article.